Commun. Comput. Phys.
doi: 10.4208/cicp.030311.090611a

Vol. **11**, No. 5, pp. 1547-1568
May 2012

# A Cluster Dynamics Model for Accumulation of Helium in Tungsten under Helium Ions and Neutron Irradiation

Y. G. Li[1], W. H. Zhou[1], R. H. Ning[1], L. F. Huang[1], Z. Zeng[1,*] and X. Ju[2]

[1] *Key Laboratory for Materials Physics, Institute of Solid State Physics, Chinese Academy of Sciences, Hefei, 230031, China.*
[2] *Department of Physics, University of Science and Technology Beijing, Beijing 100083, China.*

Received 3 March 2011; Accepted (in revised version) 9 June 2011

Communicated by Haiqing Lin

Available online 3 January 2012

**Abstract.** A cluster dynamics model based on rate theory has been developed to describe the accumulation and diffusion processes of helium in tungsten under helium implantation alone or synergistic irradiation with neutron, by involving different types of objects, adopting up-to-date parameters and complex reaction processes as well as considering the diffusion process along with depth. The calculated results under different conditions are in good agreement with experiments much well. The model describes the behavior of helium in tungsten within 2D space of defect type/size and depth on different ions incident conditions (energies and fluences) and material conditions (system temperature and existent sinks), by including the synergistic effect of helium-neutron irradiations and the influence of inherent sinks (dislocation lines and grain boundaries). The model, coded as IRadMat, would be universally applicable to the evolution of defects for ions/neutron irradiated on plasma-facing materials.

**PACS**: 02.60.Cb, 61.80.Az, 61.72.Cc, 61.72.J-

**Key words**: Cluster dynamics model, rate theory, helium and neutron irradiation, tungsten, accumulation and diffusion.

## 1 Introduction

In tokamak fusion reactors (e.g. ITER), plasma-facing materials (PFMs, e.g. Be, C and W) suffer heavy bombardment from the plasma by particles such as hydrogen isotope

*Corresponding author. *Email addresses:* ygli@theory.issp.ac.cn (Y. G. Li), whzhou@theory.issp.ac.cn (W. H. Zhou), rhning@theory.issp.ac.cn (R. H. Ning), lfhuang@theory.issp.ac.cn (L. F. Huang), zzeng@theory.issp.ac.cn (Z. Zeng), jux@ustb.edu.cn (X. Ju)

 

(H, D and T) and helium (He) ions with the energy ranging from 10 eV to several keV as well as energetic neutrons and high heat loads generated by D-T fusion reaction [1]. This process can cause damages to the metal surface, such as, erosion, sputtering, blistering, etc. [2]. Especially, He atoms injected into metals would be deeply trapped by lattice defects such as vacancies and He-vacancy complexes formed by themselves or neutrons irradiation [3], which can alter the microstructure and thus the mechanical properties of the material. On the other hand, due to their excellent thermal properties, low solubility for hydrogen and low sputtering yield, tungsten (W) based materials are termed as potential candidates for the divertor armor tiles in the future fusion reactor like ITER [2]. Therefore, the mechanisms of defects accumulation and diffusion under He ions irradiation on PFMs like W are important to estimate the damage formation and distribution, which have not been well understood.

Consequently, effects of He ions irradiation on W and other metals have been extensively investigated over a wide range of burning plasma conditions with different ion energies/fluences and system temperatures, using ion accelerators or large-sized plasma confinement devices as well as several analysis techniques [3–25]. During implantation, injected He atoms would be deeply trapped by different kinds of existing lattice defects near surface. Thus, the distribution of He atoms in W is mainly in near surface of several nms to several- tenth nms for keV He ions, while a little fraction can extend into in-bulk. It is necessary to comprehend the mechanics of He trapping and diffusion effects and the contributions by different types of He clusters in W quantitatively.

While the evolution of defects upon irradiation is by nature a multi-scale phenomenon, numerical study of defects evolution requires a multi-scale atomistic-continuum modeling approach [26, 27]. Particularly for the long-term kinetic evolution of defects, cluster dynamics (CD) [25, 28] and kinetic Monte Carlo (KMC) models [29, 30] are commonly used by requiring previous knowledge of defects created during irradiation, their mobility as well as their energetic properties [31]. These models have also been performed to the case of He ions irradiation on W, recently. Watanabe et al. [25] studied the formation of interstitial loops in W under He ions irradiation by using rate theory modeling and compared with experiment. Xu et al. [28] investigated the effects of He on the microstructure evolution in W during He and neutron irradiations based on a simple model using rate theory. Perhaps, more reliable parameters (especially the characteristic energies) or more reasonable reaction mechanisms of defects should be addressed to obtain credible results. Becquart et al. [29, 30] studied the micro-structural evolution of irradiated W with He by using an object KMC (OKMC) model based on the ab initio parameterizations. However, this model can not be applied to the case of long-range scale diffusion due to its low efficiency.

In fact, although KMC model can account for the spatial and temporal correlations, it is limited to small volumes ($\sim \mu m$), low irradiation dose (typically much less than 1 dpa) and small time scales, far from the order of practical nuclear reactor undergoing. On the contrary, CD model based on the mean-field rate theory can explore the evolution of defects over large space scales (intermediate-length) and time scales ($\sim \mu s$ to years),

which is close to those achieved experimentally. In spite of excluding of the stochastic effects/spatial correlations caused by the random nature of the cascade initiation, CD models would predict the same behavior as KMC models at least at high temperature [32], on irradiation conditions that produce a high density of defects and for materials that have a relative high density of fixed sinks [33]. Since CD models require small computational resources, they represent thus an attractive alternative to KMC approach to predict defect evolution under these conditions.

Moreover, although different types of irradiations occur simultaneously in actual fusion devices, they are used to be treated individually, such as for He or hydrogen plasma with different energies and fluxes irradiation on different PFMs [3, 4, 6, 10, 11, 13, 15, 16, 19, 25]. Recently, experimental studies have also been performed with the synergistic actions of more than one types of irradiations, such as, He irradiation with high heat loads [7, 12, 21, 24] or with different temperatures [5, 9] and hydrogen isotope-helium sequential irradiation [8, 14, 17, 18, 20, 22, 24]. It is worth mentioning that the studies of multiplier effects of He [28] or Tritium [34] plasma and neutron irradiation on W were performed by Xu et al. [28] using a simple rate theory model, which explain the formation of He/T-vacancy complexes. Therefore, it is very important to consider the synergistic effects of different irradiations and the interplay between them.

Thus, we develop a cluster dynamics model in this paper by involving different types of objects, adopting up-to-date parameters as well as complex reaction processes, considering the diffusion process along with depth and including/excluding the synergistic effects of He implantation and neutron irradiation. Furthermore, an efficient numerical method is employed to solve the thousands of equations. Our theoretical approach is a very efficient tool to simulate the dynamics processes of He in W in a long depth scale and has been coded as IRadMat. The results calculated from IRadMat enable us to improve the understanding on the accumulation and diffusion processes of He in W under the synergistic effects of He implantation and neutron irradiation related to the conditions like in ITER. IRadMat could also be generally applied to the cases of other ions (e.g. H, D, T and etc.) in other PFMs/structural materials, by using the corresponding characteristic parameters.

## 2 Simulation model

The reaction rate theory has been developed and utilized commonly for a long term, which provides relevant information on the long-time behavior of systems with different metastable states [35, 36]. Based on rate theory, a series of CD models that account for the evolution of impurities [37], solutions [25, 38–42] and/or only intrinsic defects created during irradiation [39, 43–50] have been developed in the last decades to calculate the size and space-distribution functions of defect clusters with time treated in 1-D [39, 43–50], 2-D [25, 38, 40–42] or 3-D [37] size space, under energetic electrons [40, 48, 49], neutrons [40, 42, 45, 47, 50] or plasma ions [25, 37, 38, 41, 43, 46] irradiation on different structure

metals (such as, pure iron [37,46,50], nickel [38,39], tungsten [25], stainless steels [41–45], iron alloy [40, 48], zirconium single crystals [47, 49], etc.). However, most of them are solved under steady irradiation without considering the diffusion processes of mobile defects in a long-range space scale. Recently, attempts have also been carried out to consider the effect of helium diffusion along with depth in tungsten [28] and iron [51,52], which gives an insight into the simulation of the dynamics processes of He in W in a long-range depth scale mentioned here.

The CD model used here can provide information about the roles of different migration and reaction mechanisms, as well as the diffusion processes along with depth for different defects. Several assumptions are employed as follows:

(1) The basic types of defects included in the model are self-interstitial atoms (SIAs, $I$), vacancies ($V$), helium atoms ($He$) and the formed complex clusters ($I_n$, $V_n$, $He_n$, $He_nI$, and $He_mV_n$, where $m$, $n$ is the number of defects in a loop / cluster) by binary reactions. In addition, other inherent sinks like dislocation lines ($D$) and grain boundaries ($S$) are also included.

(2) Only SIAs ($I$), di-interstitials ($I_2$), vacancies ($V$) and helium atoms ($He$) are considered to be mobile for simplification, while all other defect clusters are considered to be immobile.

(3) The reaction types assumed and the corresponding rate coefficients are listed in Table 1. For simplicity, the trap mutation effect has not been explicitly considered here. The trap mutation is defined as the process during which a He-vacancy complex containing excess helium atoms creates additional vacancies by emission of SIAs into its surrounding lattice [25], because of the existence of stress field due to the pressure of the helium bubble [53]. This is a reasonable approximation to the case of keV-He ions irradiation here for two reasons: first, it is a minor contribution by He clusters with sizes larger than about 6 whose concentration is negligible. Second, it can hardly influence the distribution of He concentrations here but just influence the existing forms of He clusters mildly. Indeed, the contributions of the trap mutation effect for the cases here are negligible as shown in the following results (Fig. 4(b) comparing with the same case in [54]) when just setting the objects of $He_mV_nI$ $(m>6)$ as $He_mV_{n-1}$ (the corresponding reaction types are also listed in Table 1).

## 2.1 Master equations

The cluster dynamical processes considered here are described with rate theory model in terms of the density/concentration of different defects along with depth for the case of synergistic effects of He implantation and neutron irradiation. The evolutions of mobile defects are described in a set of one-dimensional spatial diffusion-reaction equations by taking into account their diffusion and possible reactions with other defects, while immobile clusters clearly follow a Markovian chain process and their evolutions are described

Table 1: Reaction types and the corresponding rate coefficients.

| Reaction types | Rate coefficients |
|---|---|
| $I+V \rightleftharpoons 0$; | $k^+_{I+V}$, $G_{I/V}$ |
| $I+I_n \rightleftharpoons I_{n+1}$; | $\alpha^+_n$, $\alpha^-_{n+1}$ |
| $I+V_n \to V_{n-1}$; | $k^+_{V_n+I}$ |
| $I+He_n \rightleftharpoons He_nI$; | $k^+_{He_n+I}$, $k^-_{He_nI}$ |
| $I+He_mV_n \rightleftharpoons He_mV_{n-1}$; | $k^+_{He_mV_n+I}$, $k^-_{He_mV_{n-1}-I}(m>6)$ |
| $I_2+I_n \rightleftharpoons I_{n+2}$; | $\beta^+_n$, $\beta^-_{n+2}$ |
| $I_2+V_n \to V_{n-2}$; | $k^+_{V_n+I_2}$ |
| $I_2+He_mV_n \to He_mV_{n-2}$; | $k^+_{He_mV_n+I_2}$ |
| $V+I_n \rightleftharpoons I_{n-1}$; | $k^+_{I_n+V}$, $k^-_{I_{n-1}-V}$ |
| $V+V_n \rightleftharpoons V_{n+1}$; | $\gamma^+_n$, $\gamma^-_{n+1}$ |
| $V+He_n \rightleftharpoons He_nV$; | $k^+_{He_n+V}$, $k^-_{He_nV}$ |
| $V+He_nI \to He_n$; | $k^+_{He_nI+V}$ |
| $V+He_mV_n \rightleftharpoons He_mV_{n+1}$; | $\omega^+_n$, $\omega^-_{n+1}$ |
| $He+V_n \rightleftharpoons HeV_n$; | $k^+_{V_n+He}$, $k^-_{HeV_n}$ |
| $He+He_n \rightleftharpoons He_{n+1}$; | $\eta^+_n$, $\eta^-_{n+1}$ |
| $He+He_nI \rightleftharpoons He_{n+1}I$; | $\mu I^+_n$, $\mu I^-_{n+1}$ |
| $He+He_mV_n \rightleftharpoons He_{m+1}V_n$; | $\mu V^+_{mn}$, $\mu V^-_{(m+1)n}$ |
| $\theta+D \to D\theta$; | $k^+_{D+\theta}(\theta=I,V,He)$ |
| $\theta+S \to S\theta$; | $k^+_{S+\theta}(\theta=I,V,He)$ |

by the master equations [28, 43, 44, 48–51],

$$\frac{\partial C_\theta}{\partial t} = G_\theta + D_\theta \nabla^2 C_\theta + \sum_{\theta'} \left[ w\left(\theta',\theta\right) C_{\theta'} - w\left(\theta,\theta'\right) C_\theta \right] - L_\theta, \tag{2.1}$$

where $C_\theta$ $(\theta = I, I_2, V, X, I_n, V_n, X_n, He_nI, X_mV_n)$ is the concentration of defect of $\theta$, $G_\theta$, $D_\theta$ and $L_\theta$ $(\theta = I, I_2, V, X)$ are the production rate, the diffusion coefficient and absorption rate of different mobile defects in materials, respectively, $w(\theta',\theta)$ is the transition rate coefficient per unit concentration of a defect cluster of type $\theta'$ to a defect cluster of type $\theta$ (as list in Table 1). The four parts of the right side in Eq. (2.1) are the generation term (under He ions and neutron irradiation), the diffusion term (along with depth), the reaction terms (including forward and reverse reactions) and the absorption term (such as, the absorption by impurity, dislocation line, grain boundary, surface and etc.), respectively.

In detail, the master equations of different types of involved defects can be given as

$$\begin{aligned}\frac{\partial C_I}{\partial t} =& G_{I/V} + D_I \nabla^2 C_I - k^+_{I+V}\left(C_I C_V - C_I^{eq} C_V^{eq}\right) - 2\left(\alpha_1^+ C_I^2 - \alpha_2^- C_{I_2}\right) \\ &+ k^+_{V+I_2} C_V C_{I_2} - \sum_{n\geq 2}\left(\alpha_n^+ C_I C_{I_n} - \alpha^-_{n+1} C_{I_{n+1}}\right) - \sum_{n=2}^{N_V} k^+_{V_n+I} C_I C_{V_n}\end{aligned}$$

$$
\begin{aligned}
&-\sum_{n=1}^{N_X}\left(k^+_{X_n+I}C_IC_{X_n}-k^-_{X_nI}C_{X_nI}\right)+\sum_{n=7}^{N_X}k^-_{X_n-I}C_{X_n}\\
&-\sum_{n=1}^{N_V}\sum_{m=1}^{M_X}k^+_{X_mV_n+I}C_IC_{X_mV_n}+\sum_{n=1}^{N_V}\sum_{m=7}^{M_X}k^-_{X_mV_n-I}C_{X_mV_n}-L_I, \qquad (2.2)
\end{aligned}
$$

$$
\begin{aligned}
\frac{\partial C_{I_2}}{\partial t}=&D_{I_2}\nabla^2C_{I_2}+\left(\alpha_1^+C_I^2-\alpha_2^-C_{I_2}\right)-2\left(\beta_2^+C_{I_2}^2-\beta_4^-C_{I_4}\right)\\
&+k^+_{I_3+V}C_{I_3}C_V-\left(\alpha_2^+C_{I_2}C_I-\alpha_3^-C_{I_3}\right)\\
&-\sum_{n\geq 3}\left(\beta_n^+C_{I_2}C_{I_n}-\beta^-_{n+2}C_{I_{n+2}}\right)-\sum_{n=1}^{N_V}k^+_{V_n+I_2}C_{I_2}C_{V_n}\\
&-\sum_{n=1}^{N_V}\sum_{m=1}^{M_X}k^+_{X_mV_n+I_2}C_{I_2}C_{X_mV_n}-L_{I_2}, \qquad (2.3)
\end{aligned}
$$

$$
\begin{aligned}
\frac{\partial C_V}{\partial t}=&G_{I/V}+D_V\nabla^2C_V-k^+_{I+V}\left(C_IC_V-C_I^{eq}C_V^{eq}\right)-2\left(\gamma_1^+C_V^2-\gamma_2^-C_{V_2}\right)\\
&-k^+_{I_2+V}C_VC_{I_2}-\sum_{n\geq 3}\left(k^+_{I_n+V}C_VC_{I_n}-k^-_{I_{n-1}-V}C_{I_{n-1}}\right)-\sum_{n=2}^{N_V}\left(\gamma_n^+C_VC_{V_n}-\gamma^-_{n+1}C_{V_{n+1}}\right)\\
&-\sum_{n=1}^{N_X}\left[\left(k^+_{X_n+V}C_VC_{X_n}-k^-_{X_nV}C_{X_nV}\right)+k^+_{X_nI+V}C_VC_{X_nI}\right]\\
&-\sum_{n=1}^{N_V}\sum_{m=1}^{M_X}\left(\omega_n^+C_VC_{X_mV_n}-\omega^-_{n+1}C_{X_mV_{n+1}}\right)-L_V, \qquad (2.4)
\end{aligned}
$$

$$
\begin{aligned}
\frac{\partial C_X}{\partial t}=&G_X+D_X\nabla^2C_X-2\left(\eta_1^+C_X^2-\eta_2^-C_{X_2}\right)-\left(k_{X+I}C_XC_I-k^-_{X_nI}C_{X_nI}\right)\\
&+k^+_{XI+V}C_{XI}C_V-\sum_{n=1}^{N_V}\left(k^+_{V_n+X}C_XC_{V_n}-k^-_{V_nX}C_{V_nX}\right)\\
&-\sum_{n=2}^{N_X}\left(\eta_n^+C_XC_{X_n}-\eta^-_{n+1}C_{X_{n+1}}\right)-\sum_{n=1}^{N_X}\left(\mu I_n^+C_XC_{X_nI}-\mu I^-_{n+1}C_{X_{n+1}I}\right)\\
&-\sum_{n=1}^{N_V}\sum_{m=1}^{M_X}\left(\mu V^+_{mn}C_XC_{X_mV_n}-\mu V^-_{(m+1)n}C_{X_{m+1}V_n}\right)-L_X, \qquad (2.5)
\end{aligned}
$$

$$
\begin{aligned}
\frac{\partial C_{I_n}}{\partial t}\Big|_{3\leq n\leq N_I}=&-\left(\alpha_n^+C_IC_{I_n}-\alpha^-_{n+1}C_{I_{n+1}}\right)+\left(\alpha^+_{n-1}C_IC_{I_{n-1}}-\alpha_n^-C_{I_n}\right)\\
&-\left(\beta_n^+C_{I_2}C_{I_n}-\beta^-_{n+2}C_{I_{n+2}}\right)+\left(\beta^+_{n-2}C_{I_2}C_{I_{n-2}}-\beta_n^-C_{I_n}\right)\\
&-\left(k^+_{I_n+V}C_VC_{I_n}-k^-_{I_{n-1}-V}C_{I_{n-1}}\right)+\left(k^+_{I_{n+1}+V}C_VC_{I_{n+1}}-k^-_{I_n-V}C_{I_n}\right), \qquad (2.6)
\end{aligned}
$$

$$
\begin{aligned}
\frac{\partial C_{V_n}}{\partial t}\Big|_{2\leq n\leq N_V}=&-k^+_{V_n+I}C_IC_{V_n}+k^+_{V_{n+1}+I}C_IC_{V_{n+1}}-k^+_{V_n+I_2}C_{I_2}C_{V_n}\\
&+k^+_{V_{n+2}+I_2}C_{I_2}C_{V_{n+2}}-\left(\gamma_n^+C_VC_{V_n}-\gamma^-_{n+1}C_{V_{n+1}}\right)\\
&+\left(\gamma^+_{n-1}C_VC_{V_{n-1}}-\gamma_n^-C_{V_n}\right)-\left(k^+_{V_n+X}C_XC_{V_n}-k^-_{XV_n}C_{XV_n}\right), \qquad (2.7)
\end{aligned}
$$

$$\begin{aligned}\frac{\partial C_{X_n}}{\partial t}|_{2\le n\le N_X} =& -\left(k^+_{X_n+I}C_IC_{X_n}-k^-_{X_nI}C_{X_nI}\right)-\left(k^+_{X_n+V}C_VC_{X_n}-k^-_{X_nV}C_{X_nV}\right)\\ &+k^+_{X_nI+V}C_VC_{X_nI}+k^+_{X_nV+I}C_IC_{X_nV}+k_{X_nV_2+I_2}C_{I_2}C_{X_nV_2}\\ &-\left(\eta^+_nC_XC_{X_n}-\eta^-_{n+1}C_{X_{n+1}}\right)+\left(\eta^+_{n-1}C_XC_{X_{n-1}}-\eta^-_nC_{X_n}\right)\\ &-k^-_{X_n-I}C_{X_n}|_{n>6}\,,\end{aligned} \tag{2.8}$$

$$\begin{aligned}\frac{\partial C_{X_nI}}{\partial t}|_{1\le n\le N_X} =& \left(k^+_{X_n+I}C_IC_{X_n}-k^-_{X_nI}C_{X_nI}\right)-k^+_{X_nI+V}C_VC_{X_nI}\\ &-\left(\mu I^+_nC_XC_{X_nI}-\mu I^-_{n+1}C_{X_{n+1}I}\right)+\left(\mu I^+_{n-1}C_XC_{X_{-1}}-\mu I^-_nC_{X_nI}\right),\end{aligned} \tag{2.9}$$

$$\begin{aligned}\frac{\partial C_{X_mV}}{\partial t}|_{1\le m\le M_X} =& -\left(k^+_{X_mV+I}C_IC_{X_mV}-k^+_{X_mV_2+I}C_IC_{X_mV_2}\right)-\left(\omega^+_1C_VC_{X_mV}-\omega^-_2C_{X_mV_2}\right)\\ &-\left(k^+_{X_mV+I_2}C_{I_2}C_{X+mV}-k^+_{X_mV_3+I_2}C_{I_2}C_{X_mV_3}\right)\\ &-\left(\mu V^+_{m1}C_XC_{X_mV}-\mu V^-_{(m+1)1}C_{X_{m+1}V}\right)\\ &+\left(\mu V^+_{(m-1)1}C_XC_{X_{m-1}V}-\mu V^-_{m1}C_{X_mV}\right)\\ &+\left(k^-_{X_m-I}C_{X_m}-k^-_{X_mV-I}C_{X_mV}\right)|_{m>6}\,,\end{aligned} \tag{2.10}$$

$$\begin{aligned}\left.\frac{\partial C_{X_mV_n}}{\partial t}\right|_{\substack{2\le n\le N_V\\1\le m\le M_X}} =& -\left(k^+_{X_mV_n+I}C_IC_{X_mV_n}-k^+_{X_mV_{n+1}+I}C_IC_{X_mV_{n+1}}\right)\\ &-\left(k^+_{X_mV_n+I_2}C_{I_2}C_{X_mV_n}-k^+_{X_mV_{n+2}+I_2}C_{I_2}C_{X_mV_{n+2}}\right)\\ &-\left(\omega^+_nC_VC_{X_mV_n}-\omega^-_{n+1}C_{X_mV_{n+1}}\right)+\left(\omega^+_{n-1}C_VC_{X_mV_{n-1}}-\omega^-_nC_{X_mV_n}\right)\\ &-\left(\mu V^+_{mn}C_XC_{X_mV_n}-\mu V^-_{(m+1)n}C_{X_{m+1}V_n}\right)\\ &+\left(\mu V^+_{(m-1)n}C_XC_{X_{m-1}V_n}-\mu V^-_{mn}C_{X_mV_n}\right)\\ &-\left(k^-_{X_mV_n-I}C_{X_mV_n}-k^-_{X_mV_{n-1}-I}C_{X_mV_{n-1}}\right)|_{m>6}\,,\end{aligned} \tag{2.11}$$

where $X=He$ in Eqs. (2.2)-(2.11), $C^{eq}_\theta$ $(\theta=I,V)$ are the concentrations of SIAs and vacancies at thermodynamical equilibrium, and $N_I,N_V,N_X,M_X$ are the maximum size of interstitial loops, vacancy and He atom clusters as well as He atoms in $He_mV_n$ complexes, respectively. All equations (Eqs. (2.2)-(2.11)) are solved for a set of depth points of $N_z$.

## 2.2 Rate coefficients

The rate coefficients listed in Table 1 describe the physical production rates and the rates of capture and emission of point defects by defect clusters [48–50]. These processes include the production and recombination of $I-V$ point defects and the reactions of $I_n-\theta|_{\theta=I,I_2,V}$, $V_n/He_n/He_mV_n-\theta|_{\theta=I,I_2,V,He}$, $He_nI-\theta|_{\theta=V,He}$ and $D/S-\theta|_{\theta=I,V,He}$.

### 2.2.1 Production and recombination of $I-V$ point defects

The production rate of Frenkel-pairs by He implantation and neutron irradiation, $G_{I/V}$ $\left(dpa\ s^{-1}\right)$, is simply treated as that: a uniform rate caused by neutron irradiation is introduced across the whole domain, while the rate distribution near surface caused by He implantation is estimated by TRIM-code [55].

The recombination rate of SIA and vacancy point defects is given by,

$$k^+_{I+V}=4\pi r_{IV}\left(D_I+D_V\right), \tag{2.12}$$

where $r_{IV}$ is the recombination radius, $D_I$ and $D_V$ are the diffusion coefficients of SIA and vacancy point defects, respectively, and expressed in terms of Arrhenius form for thermally activated events:

$$\begin{cases} D_I=D_{I_0}\exp\left(-E^m_I/k_BT\right), \\ D_V=D_{V_0}\exp\left(-E^m_V/k_BT\right), \end{cases} \tag{2.13}$$

here, $D_{I_0}$ and $D_{V_0}$ are the pre-exponential factors of the point defects, $k_B$ is the Boltzmann constant.

### 2.2.2 Rate coefficients for $I_n-\theta|_{\theta=I,I_2,V}$

The rate of absorption of point defects $(I,I_2,V)$ by dislocation loops $(I_n)$ is usually given by

$$\begin{cases} \alpha^+_n=2\pi r_{I_n}Z^I_{I_n}D_I, \\ \beta^+_n=2\pi r_{I_n}Z^{I_2}_{I_n}D_{I_2}, \\ k^+_{I_n+V}=2\pi r_{I_n}Z^V_{I_n}D_V, \end{cases} \tag{2.14}$$

where $r_{I_n}$ is the loop radius, which is given by making the assumption that the SIA point defects agglomerate to form dislocation/interstitial loops:

$$r_{I_n}=\sqrt{nV_{at}/\pi b}, \tag{2.15}$$

where $V_{at}=a_0^3/2$ is the atomic volume for bcc metals like W, $b$ is the Burger vector of the dislocation loop, $Z^\theta_{I_n}|_{\theta=I,I_2,V}$ is an efficiency factor that makes it possible to take the defect-dislocation elastic interaction and also the toroidal shape of the loop into account [49]:

$$Z^\theta_{I_n}=Z^\theta_D\max\left\{\frac{2\pi}{\ln\left(8r_{I_n}/r_p\right)},1\right\}, \tag{2.16}$$

where $Z^\theta_D$ is the capture efficiency factor of point defect $\theta$ by dislocation loops, $r_p$ is the pipe radius of dislocation loops and is usually taken equal to $2b$.

For the case of point defects emitted from dislocation loops, the rate coefficients are obtained by the detail balance:

$$\begin{cases} \alpha_n^- = 2\pi r_{I_{n-1}} Z^I_{I_{n-1}} D_I \exp\left(-E^b_{I_n-I}\Big/k_BT\right)\Big/V_{at}, \\ \beta_n^- \cong 2\pi r_{I_{n-1}} Z^I_{I_{n-1}} D_{I_2} \exp\left(-E^b_{I_n-I_2}\Big/k_BT\right)\Big/V_{at}, \\ k^-_{I_{n-1}-V} = 2\pi r_{I_{n-1}} Z^V_{I_{n-1}} D_V \exp\left(-E^b_{I_n-V}\Big/k_BT\right)\Big/V_{at}, \end{cases} \tag{2.17}$$

where $E^b_{I_n-\theta}|_{\theta=I,I_2,V} = E^f_\theta - \left(E^f_{I_n} - E^f_{I_n-\theta}\right)$ are the binding energies of point defects $(I, I_2, V)$ with dislocation loops, which can be estimated by the capillary law approximation [30, 48, 49],

$$\begin{cases} E^b_{I_n-I} = E^f_I + \frac{E^b_{I_2}-E^f_I}{2^{2/3}-1}\left[n^{2/3}-(n-1)^{2/3}\right], \\ E^b_{I_n-I_2} = 2E^f_I - E^b_{I_2} - \left(2E^f_I - E^b_{I_n-I} - E^b_{I_{n-1}-I}\right), \\ E^b_{I_n-V} = E^f_V + \frac{E^f_I-E^b_{I_2}}{2^{2/3}-1}\left[n^{2/3}-(n-1)^{2/3}\right], \end{cases} \tag{2.18}$$

where $E^f_\theta|_{\theta=I,V,I_n}$ are the formation energies of SIAs, vacancies and dislocation loops, and $E^b_{\theta_2}|_{\theta=I,V}$ are the binding energies of $I_2$ and $V_2$.

### 2.2.3 Rate coefficients for $V_n-\theta|_{\theta=I,I_2,V,He}$

The rate of absorption of point defects $(I, I_2, V, He)$ by spherical vacancy clusters is calculated according to the assumption of a diffusion limited regime

$$\begin{cases} k^+_{V_n+\theta}|_{\theta=I,I_2,He} = 4\pi r_{V_n} D_\theta, \\ \gamma^+_n = 4\pi r_{V_n} D_V, \end{cases} \tag{2.19}$$

where $r_{V_n}$ is the cluster $(V_n)$ radius

$$r_{V_n} = \left(\frac{3nV_{at}}{4\pi}\right)^{1/3} + r_0, \tag{2.20}$$

with $r_0 = \sqrt{3}a_0/4$.

Only the point defects of $V$ and $He$ are assumed to be emitted from a vacancy cluster here. Their rate coefficients are also obtained by the detail balance:

$$\begin{cases} \gamma^-_n = 4\pi r_{V_{n-1}} D_V \exp\left(-E^b_{V_n-V}\Big/k_BT\right)\Big/V_{at}, \\ k^-_{V_n-He} = 4\pi r_{V_{n-1}} D_{He} \exp\left(-E^b_{V_n-He}\Big/k_BT\right)\Big/V_{at}, \end{cases} \tag{2.21}$$

where $E^b_{V_n-V}$ and $E^b_{V_n-He}$ are the binding energies of a vacancy cluster with a vacancy and a He atom, respectively,

$$E^b_{V_n-V} = E^f_V + \frac{E^b_{V_2}-E^f_V}{2^{2/3}-1}\left[n^{2/3}-(n-1)^{2/3}\right], \tag{2.22}$$

and $E^b_{V_n-He}$ can be obtained from ab initio or molecular dynamics (MD) calculation for small clusters and extrapolated for the larger size ones like in [29,30].

#### 2.2.4 Rate coefficients for $He_n/He_mV_n-\theta|_{\theta=I,I_2,V,He}$ and $He_nI-\theta|_{\theta=V,He}$

For the cases of $He_n/He_mV_n-\theta|_{\theta=I,I_2,V,He}$ and $He_nI-\theta|_{\theta=V,He}$, the reaction rate coefficients ($k^+_{He_n+I}$, $k^+_{He_n+V}$, $k^-_{He_nV}$,$\eta^+_n$, $\eta^-_{n+1}$; $k^+_{He_mV_n+I}$, $k^+_{He_mV_n+I_2}$, $\omega^+_n$, $\omega^-_{n+1}$, $\mu V^+_{mn}$, $\mu V^-_{(m+1)n}$; $k^+_{He_nI+V}$, $\mu I^+_n$, $\mu I^-_{n+1}$) are treated equally to those for $V_n-\theta|_{\theta=I,I_2,V,He}$.

#### 2.2.5 Rate coefficients for absorption of point defects by dislocation lines and grain boundaries

The absorption rates $L_\theta = k^+_{D+\theta}+k^+_{S+\theta}|_{\theta=I,V,He}$ of point defects include the contributions from dislocation lines $k^+_{D+\theta}|_{\theta=I,V,He}$ and grain boundaries $k^+_{S+\theta}|_{\theta=I,V,He}$, which can be estimated by taking account of the dislocation line density $\rho_D$ and the grain size $d$, respectively [48,49].

The absorption rate $k^+_{D+\theta}|_{\theta=I,V,He}$ of mobile defects of type $\theta$ by per unit of length of dislocation lines is

$$k^+_{D+\theta}|_{\theta=I,V,He} = \rho_D Z^\theta_D D_\theta C_\theta, \tag{2.23}$$

where $Z^\theta_D$ is also a dimensionless factor representing the absorption efficiency of point defects by the dislocation lines.

The absorption rate $k^+_{S+\theta}|_{\theta=I,V,He}$ of the mobile defects of type $\theta$ by grain boundaries is given by

$$k^+_{S+\theta}|_{\theta=I,V,He} = S^{sk}_\theta D_\theta C_\theta, \tag{2.24}$$

where $S^{sk}_\theta = \left(S^{sc}_\theta\right)^{1/2} H$, with $S^{sc}_\theta$ the sum of the sink strengths of all the sinks but the grain boundary and $H = 6/d$ for a grain boundary.

### 2.3 Numerical methods

The evolution of cluster size is then obtained through numerical resolution of a set of partial differential equations (PDEs). However, the interstitial loops considered here contain a large number of SIAs (typically $\sim 10^4$ here), which would exceed the current capability of computers. In order to extend this limit and increase the computation efficiency, for larger sizes of interstitial loops, the discrete master equation is usually transformed into a continuous Fokker-Plank type equation by applying a second-order Taylor series expansion [43,56]. Here, only the reaction types of SIAs with interstitial loops ($I_n-I$) are included for simplification. Indeed, this is a reasonable approximation for that the contribution of the reaction types $I_n-I_2$ is negligible as shown in our test samples below. Thus, Eq. (2.6) for the cluster size $x$ larger than a certain number $N$ can be replaced by [43,56],

$$\frac{\partial C(x,t)}{\partial t} = \frac{\partial}{\partial x}\left(-F(x,t)C(x,t)+\frac{1}{2}\frac{\partial}{\partial x}D(x,t)C(x,t)\right), \quad x>N, \tag{2.25}$$

where

$$\begin{cases} F(x,t)=\kappa(x,t)-\lambda(x,t), \\ D(x,t)=\kappa(x,t)+\lambda(x,t), \end{cases} \tag{2.26}$$

are the point defect net bias flux and point defect average diffusion flux, respectively, with

$$\begin{cases} \kappa(x(n),t)\cong\alpha_n^+ C_I(t)+k_{In-V}^-, \\ \lambda(x(n),t)\cong\alpha_n^- +k_{I_n+V}^+ C_V(t). \end{cases} \tag{2.27}$$

Here, $n$ is the integer part of $x$, that is, the approximated number of point defects in loops at size of $x$.

The combined set of equations (the discrete master equation and the continuous Fokker-Plank equation) can be solved numerically as in [56], where Turkin and Bakai considered several different well-known numerical methods traditionally used and further proposed a new realization of the hybrid approach which is rather simple and straightforward methodologically. A much simpler non-adaptive non-uniform mesh scheme is used, where the mesh spacing varies smoothly in a preset way across the computational domain. The following relationship for mesh points $x_i$ and mesh spacings $\Delta x_i$ are employed,

$$\begin{cases} x_1=1, \\ x_i=x_{i-1}+\Delta x_i, \quad 2\le i\le M, \\ \Delta x_i=\begin{cases} 1, & \text{for } 2\le i\le N, \\ \Delta x_{i-1}\exp(\varepsilon), & \text{for } N\le i\le M, \end{cases} \end{cases} \tag{2.28}$$

where $M$ is large enough to fulfill the boundary condition $C(x_M)=0$, $0<\varepsilon\ll 1$ is a small parameter which controls the mesh spacing. It is easy to find the explicit relationship between mesh point $x_i$ and point number $i$,

$$i=N+\frac{1}{\varepsilon}\ln\left(1+\frac{\exp(\varepsilon)-1}{\exp(\varepsilon)}(x_i-N)\right), \quad x\ge N. \tag{2.29}$$

The PDEs are transformed approximately to conservative finite difference equations on the non-uniform mesh by using central finite differencing, i.e., the set of ordinary differential equations (ODEs),

$$\begin{aligned} \frac{dC_i(t)}{dt}=\frac{1}{\Delta x_{i+1}+\Delta x_i}\Big[&-(F_{i+1}C_{i+1}-F_{i-1}C_{i-1}), \\ &+\left(\frac{D_{i+1}C_{i+1}-D_iC_i}{\Delta x_{i+1}}-\frac{D_iC_i-D_{i-1}C_{i-1}}{\Delta x_i}\right)\Big]. \end{aligned} \tag{2.30}$$

For the diffusion term related to mobile defects in Eqs. (2.2)-(2.5), clearly it is more convenient and efficient to use a nonuniform mesh because the values of $C_\theta$ attenuate

with depth $z$ over a large scale. Thus, the diffusion term at point $j$ can then be expressed by a finite difference approximation with a non-uniform mesh as [57],

$$\frac{\partial^2 C_\theta^j}{\partial z^2}|_{\theta=I,I_2,V,X} = \frac{2}{(1+\delta)h}\left(\frac{C_\theta^{j+1}-C_\theta^j}{\delta h} - \frac{C_\theta^j - C_\theta^{j-1}}{h}\right), \tag{2.31}$$

where $h$ is the interval of the last mesh and $\delta > 1$ is a parameter controlling the mesh spacing to increase with point number of $j$.

Furthermore, in order to account for He desorption, the first-order boundary conditions in both surface and sufficient depth are used [51]. Here, we assume that the flux of He atoms at the surface is proportional to the concentration of He atoms and only limited by diffusion. This approximation is reasonable enough for that the migration energy of He is only 0.06 $eV$ in W, which can be regarded as a free diffusion. Otherwise, we consider the surface as the sink for $I$, $I_2$, and $V$ in our model.

Here, the system of ODEs is solved by using *lsoda* subroutine packages [58], which is well known as a liver-more solver for ODEs based on the explicit predictor-corrector method with an automatic switch for stiff and non-stiff problems. In practice, the parameters are set as $n \sim$ hundreds, $N_v \sim$ several and $N_x, M_x, N_z \sim$ tenths in general, by considering their respective precipitate size mentioned here. Thus the total number of the ODEs is estimated by $(N_I + N_v + N_x + (N_v * M_x)) * N_z$, typically in the order of $\sim 10^3$ here. Our code is efficient enough that no more than several hours are necessary for the most time-consuming input condition when using a modern personal computer.

## 3 Results and discussions

It should be noted that in order to obtain more reliable results, the parameters must be carefully chosen. We present the recommended parameters here by considering the published values from experiments or ab initio/MD calculations as listed in Table 2.

The characteristic energies such as formation energy ($E_\theta^f|_{\theta=I,V,He}$), migration energy ($E_\theta^m|_{\theta=I,V,He}$) and binding energy ($E_{\theta'_n-\theta}^f|_{\theta',\theta=I,V,He}$) are the critical parameters for reaction dynamics and must be considered correctly. By comparing different sources of data obtained from experiments and calculations, the energies used here for point defects and binary clusters in W are also listed in Table 2. While the binding energies of mobile point defects ($I, I_2, V, X$) with different types of large loops/clusters can be obtained by the capillary law approximation (as in Eqs. (2.18) and (2.22)) or by atomic-scale calculations, as shown in Fig. 1. For dislocation loops with large sizes $n$, the values derived from Eq. (2.18) with $E_I^f = 9.466\ eV$ and $E_{I_2}^b = 2.12\ eV$ for $E_{I_n-I}^b$ are in good agreement with ab initio calculated ones and also with the expression given by the elasticity theory of

Table 2: Parameters used in the case of He atoms and neutrons irradiated on W.

| | Symbol | Value | Refs. |
|---|---|---|---|
| He beam intensity | $I_{He}$ | $10^{18}-10^{22}m^{-2}s^{-1}$ | [28,59] |
| Temperature | $T$ | $300K$,$873K$ | - |
| Point defect creation rate | $G_{I/V}$ | $10^{-6}dpa\ s^{-1}$ | [28] |
| Lattice parameter | $a_0$ | $3.1652\overset{\circ}{A}$ | [60] |
| He radius | $r_{He}$ | $0.49\overset{\circ}{A}$ | - |
| Burgers vector | $b$ | $2.74\overset{\circ}{A}$ | [60] |
| Recombination radius | $r_{IV}$ | $4.65\overset{\circ}{A}$ | Estimated |
| Dislocation line density | $\rho_D$ | $10^{12}m^{-2}$ | [61] |
| Grain size | $d$ | $10\mu m$ | - |
| Interstitial pre-exponential factor | $D_{I_0}$ | $10^{-8}m^2s^{-1}$ | [25,28,30] |
| Vacancy pre-exponential factor | $D_{V_0}$ | $10^{-4}m^2s^{-1}$ | Assumed |
| He pre-exponential factor | $D_{He_0}$ | $10^{-8}m^2s^{-1}$ | [25,28,30] |
| SIA/dislocation elastic interaction | $Z_D^I$ | 1.2 | [49] |
| V/dislocation elastic interaction | $Z_D^V$ | 1.0 | [28,49] |
| He/dislocation elastic interaction | $Z_D^{He}$ | 1.0 | [28] |
| Formation energy of SIA | $E_I^f$ | $9.466\ eV$ | [62] |
| Formation energy of Vacancy | $E_V^f$ | $3.80\ eV$ | [62,63] |
| Formation energy of He | $E_{He}^f$ | $4.0\ eV$ | [30] |
| Migration energy of SIA | $E_I^m$ | $0.013\ eV$ | [64] |
| Migration energy of Vacancy | $E_V^m$ | $1.66\ eV$ | [65] |
| Migration energy of He | $E_{He}^m$ | $0.06\ eV$ | [66] |
| Binding energy of $I_2$ | $E_{I_2}^b$ | $2.12\ eV$ | [30] |
| Binding energy of $V_2$ | $E_{V_2}^b$ | $0.6559\ eV$ | [65,67] |
| Binding energy of $He_2$ | $E_{He_2}^b$ | $1.02\ eV$ | [30] |
| Binding energy of $He_n-I$ | $E_{He_n-I}^b$ | $0.94\ eV$ | [29,30] |
| Binding energy of $He_mV_n-I$ | $E_{He_mV_n-I}^b$ | $0.7\ eV\,(m>6)$ | Estimated [25] |

dislocations with neglecting the small edge core term (Fig. 1(a)) [60],

$$\begin{cases} E_{I_n}^f = 2\pi r_n \frac{\mu b^2}{4\pi(1-\nu)}\left(\ln\frac{4r_n}{\rho}-1\right), \\ E_{I_n-I}^b = E_I^f - \left(E_{I_n}^f - E_{I_{(n-1)}}^f\right), \end{cases} \tag{3.1}$$

where $r_n$ is the loop radius, $\mu$ (160 GPa for W) is the shear modulus, $\nu$ (0.28 for W) is the Poisson's ratio and $\rho$ (0.14 for W) is the dislocation core parameter. The MD calculation results [67] including the influence of high temperature for vacancy and the ab initio calculation results [29,30] for He atom were used respectively and extended with the capillary law approximation for large clusters, as shown in Fig. 1(b). The binding energies of a He atom/vacancy with $He_mV_n$ complexes obtained by ab initio calculations

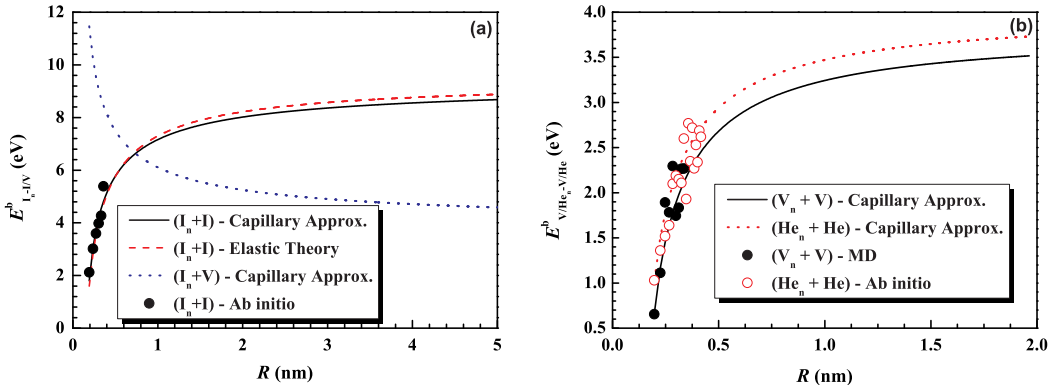


Figure 1: Binding energies of (a) a SIA/vacancy with an interstitial loop, (b) a vacancy (He atom) with a vacancy (He) cluster for W versus the size of the cluster calculated by the capillary law approximation/elastic theory [60] and obtained from MD [67]/ab initio calculations [29, 30].

for clusters up to size 23 have been presented in [30]. For larger size clusters, the data were extrapolated. In this model, the mixed SIA-He clusters ($He_nI$) are also considered, where the corresponding binding energy is set equal to 0.94 $eV$ and is independent on the cluster size $n$ [29,30]. Moreover, the binding energy of a SIA with a He-vacancy complex ($He_mV_n|_{m\geqslant 6}$)) due to the trap mutation effect is estimated to be around 0.7 $eV$, by fitting the experimental results [25].

Our model is verified by comparing with the experiments [3, 4, 7, 9, 68] as shown in Fig. 2. The He atom (apa) and damage (dpa) distributions in W determined by TRIM-code [55] are used as the initial distributions of point defects in the calculations and are also plotted together for comparison. The calculating conditions are set by concerning the experimental details as the following. For the case of 1.5 $keV$, the experiment [3] considers the depth profile of He in W bombarded by charge exchange (CX)-He atoms during large helical device (LHD) He discharges. Generally the typical plasma parameters are as the energy of $0.7-1.7$ $keV$ and the density of $0.3-8.1\times10^{19}$ $m^{-3}$. While the total duration time is 87 $s$ and the temperature of the probe head during exposure is stayed almost constant near room temperature. Additionally by comparing the evolution of microstructure with the reference data, the estimated flux is $\sim10^{19}$ $m^{-2}s^{-1}$ and incidence energy is about $1-2$ $keV$. Furthermore, by considering the elastic recoil detection (ERD) depth profile of retained He atoms in W after exposed to He discharges, the majority CX-He bombarding the first wall holds the estimated energy of a little more than 1 $keV$. Thus, the calculation conditions are taken as follows: The He plasma with a mean energy of 1.5 $keV$ and a flux of $4.0\times10^{19}$ $m^{-2}s^{-1}$ bombard W bulk with temperature of 300 $K$ for a duration time of 87 $s$. Obviously, seen from Fig. 2(a), the calculated depth profile (with the average penetration depth of $\sim11$ $nm$) of He in W is comparable to the experimental one (with the average penetration depth of $\sim13$ $nm$). For the case of 8 $keV$, the normal incidence He ions with energy of 8 $keV$ and fluence of $5\times10^{21}$ $m^{-2}$ implanted in W at 300 $K$, the experimental settings [7], are used, which leading to the fact that the calculated depth

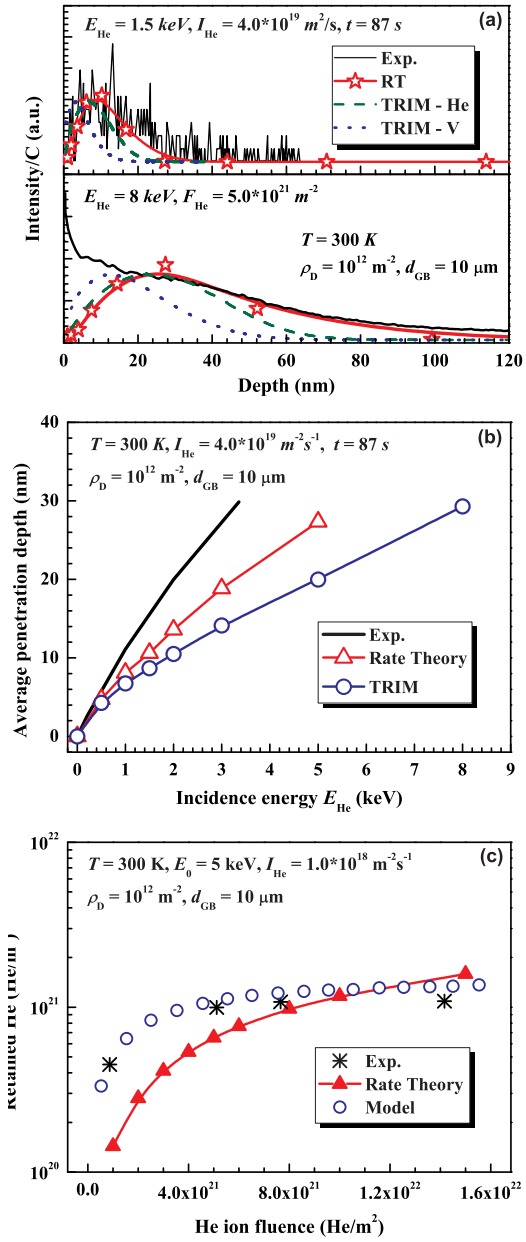


Figure 2: Comparison of calculated results and experimental ones: (a) Depth profiles of retained He atoms in W under He ions irradiation with mean energy of 1.5 $keV$ and fluence of $3.5\times10^{21}$ $m^{-2}$ [3] and with energy of 8 $keV$ and fluence of $5.0\times10^{21}$ $m^{-2}$ [7] respectively at 300 K. Inject He atom (apa) and damage (dpa) profiles calculated by TRIM-code [55] are also plotted together for comparison. (b) The average penetration depth as a function of He incident energy with the experimental one [3] and the one estimated by TRIM-code after W exposed to the He plasma with fluence of $3.5\times10^{21}$ $m^{-2}$. (c) Amount of retained He atoms versus He ions fluence in W with experimental [4, 9] and simulation results [68] for He with energy of 5 $keV$ at nonmoral incidence. The density of dislocation lines and diameter of grain boundaries in W are set as $10^{12}$ $m^{-2}$ and 10 $\mu m$ respectively for all the cases.

profile is in good agreement with the residual gas analysis (RGA) depth profile of He in W, as shown in Fig. 2(a). Generally, two effects control the depth distribution profile of He in W, that is, the trapping and diffusion effects. The competition of these two effects makes the profiles have a peak (located at about 9 - 10 nm and 25 nm for the two cases, respectively) and a long tail beyond the projected range. In addition, the average penetration depth of injected He in W as a function of incidence energy is compared with the experimental one [3] and the projection range calculated by TRIM-code (Fig. 2(b)) in which the currents are consistent with each other. Furthermore, retention of He in near surface of W was usually mentioned, for example, by the experiments under the implantation of He ions with different energies and system temperatures [4, 9] as well as a simulation study based on a ACAT-DIFFUSE code with assumed parameters [68]. Here, the amount of He retained versus He ions fluence in W for He normal implantation with an energy of 5 $keV$ is given in Fig. 2(c) and compared with the experimental [4, 9] and simulated ones [68]. In spite of including various kinds of complex influence factors (such as, multiform micro-structures of W, different experimental conditions, complexity and assumptions of the model, etc.), a reasonable agreement has been obtained without any adjusted parameters, which further verifies our model quantitatively.

Various complicated factors, such as, approximations introduced in the model and measurement errors from different special experimental conditions, can cause our calculated results to deviate from the experimental ones. As shown in Fig. 2(a) and (b), the calculated penetration depthes are somewhat undervalued here comparing to the experimental ones, which would be due to the neglected mobility of larger defects and the inaccuracy more or less of the parameters of defects used in the model, or due to the estimated bias of the experimental conditions and errors in measurement. A considerable deviation near surface for the case of 8 $keV$ in Fig. 2(a) would mainly come from the adsorption of He atoms by W surface in the experiment and partly from the choice of the boundary condition on the system surface in the calculation. Furthermore, for the amount of retained He in W versus He fluence (Fig. 2(c)), if taking no account of the errors in measurement, the main deviation of our calculation from the experiment would be mainly attribute to the immutable He diffusion coefficient in the damaged region near surface while the diffusion coefficient would increase during He ions irradiation with high fluence [68].

In the following, we consider new features of our model when applying to study the accumulation and diffusion of He in W for different typical cases, such as, describing the He concentrations within the 2D space of defect type/size and depth, including the synergistic effect of He implantation and neutron irradiation, taking into account of the influence of inherent sinks (dislocation lines (DLs) and grain boundaries (GBs)), etc.

Generally, the injected He ions in W would be scattered by the lattice atoms and slowed down/accumulated instantaneously. Associated damages in space (such as Franker-pairs) would be produced during He atoms drifting and slowing down, for He ions implantation with incident energy larger than 400 $eV$ for the case of W (above-threshold value for the displacement damage). This process is just attributed to the kinetics en-

ergy loss of injected He atoms and have been treated reasonably by TRIM-code [55]. On the other hand, the deposited He atoms would diffuse (with very low migration energy of 0.06 $eV$) due to the concentration gradient of them, and be trapped by the lattice defects such as vacancies and He-vacancy complexes instantaneously. The (drift-) diffusion effect makes the He atoms extend to a long range, while the trapping effect by defects makes the He atoms accumulate to form large clusters (i.e. $He_n$,$He_nI$,$He_mV_n$) at very near surface. Indeed, the competition of these two effects requires the evolution of He in W describing within the 2D space of defect type/size and depth, which has been fundamentally treated in our model.

Fig. 3 gives the concentrations of He atoms ($He_n-All$) as well as respective types of He clusters ($He_n$,$He_nI$,$He_mV_n$) and the absorption of inherent sinks (i.e. DLs and GBs) along with depth and defect size quantitatively, for a typical case of He ions with an incident energy of 1.5 $keV$ and a fluence of $3.5\times10^{21}$ $m^{-2}$ irradiated on W at 300 K. As shown in Fig. 3(a), it is reasonable as discussed above that the He concentrations along with depth has a peak near surface due to the deep trapping effect by intrinsic defects and self-trapping, while it is nearly a diffusion process of He atoms far from surface in spite of existing the minor self-trapping and absorption by the uniform inherent sinks. Here, $n/m$ denotes the sum of the same type of He clusters from 1 to $n/m$. The concentration of He mainly comes from He clusters such as $He_nI$ and partly from $He_n$,$He_mV_n$ near surface, as shown in the insert of Fig. 3(a). In addition, the cluster size distributions of different types of defects are evolving during He ions irradiation. The typical cluster size distributions of different types of He defects can also be represented by our model as shown in Fig. 3(b). The concentrations for different types of He clusters here denote the sums of the same types though the whole depth. Also, $He_nI$ clusters (around 67% of $He_n-All$) dominate the He clusters concentration while $He_n$ and $He_mV_n$ clusters (about 16% and 17% of $He_n-All$, respectively) are the minor parts, which are consistent with the depth distributions as shown in Fig. 3(a). The most frequent sizes of $He_n$ and $He_mV_n$ are typically less than 5 while the size of $He_nI$ clusters can grow much bigger than several tens. This current is similar to the case in [30]. Clearly, the ratios contributed by different types of He clusters are related directly to their respective initial concentrations, corresponding rate coefficients and motilities of different types of defects.

Corresponding to the conditions of PFMs in fusion devices, the synergistic irradiations of ions and neutron practically occur, other than the cases mentioned above. In [54], by using this model, we have considered the processes of accumulation and diffusion of He in neutron irradiated W (treated as a single crystal there as usual [28], without considering the absorption of DLs and GBs), for two typical cases of He plasma (with higher energy and lower flux for the first wall and with lower energy and higher flux for the divertor, respectively) as well as a uniform damages produced by neutron irradiation in contrast to the surface located injected He atoms and associated damages. Indeed, the concentrations of He clusters have the similar behavior even after considering (Fig. 4(a)) the influences of DLs and GBs (typically, the dislocation density of $10^{12}$ $m^{-2}$ and the grain diameter of 10 $\mu m$ are used). There is a shoulder peak at about 1 $\mu m$ with neutron irra-

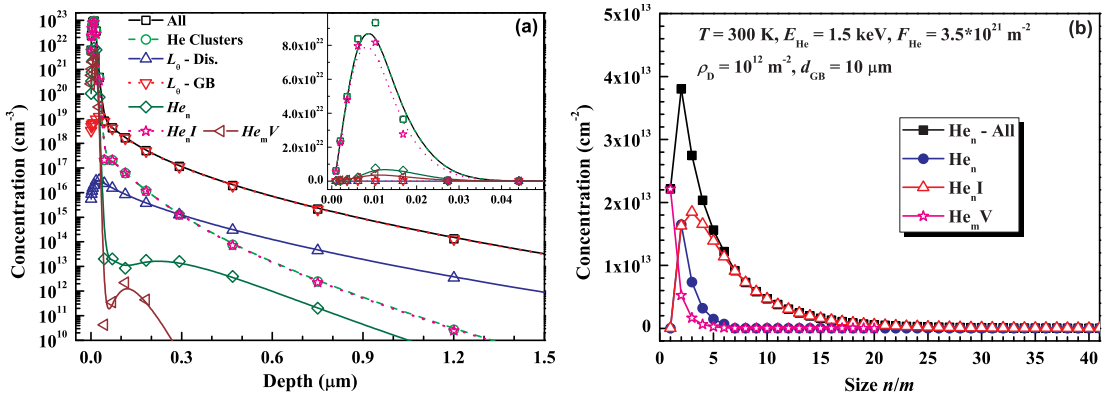


Figure 3: (a) Depth and (b) size dependence of He concentrations in W attributed to different types of He under He ions implantation with energy of 1.5 $keV$ and fluence of $3.5\times10^{21}$ $m^{-2}$ at 300 $K$. The density of dislocation lines and diameter of grain boundaries in W are set as $10^{12}$ $m^{-2}$ and 10 $\mu m$, respectively.

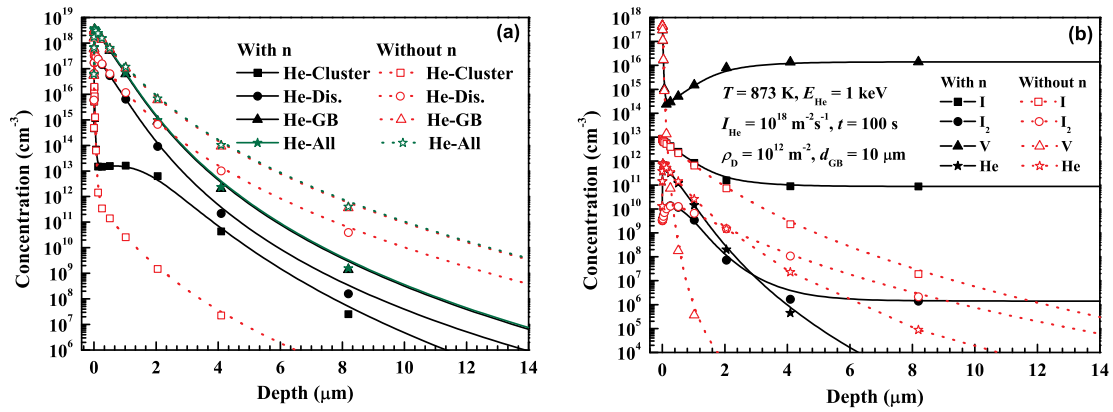


Figure 4: (a) Depth dependence of He concentrations in W attributed to different types of He under He plasma with energy of 1 $keV$ and flux of $10^{18}$ $m^{-2}s^{-1}$ and with/without synergistic neutron irradiation at 873 $K$ and 100 $s$. (b) The corresponding concentrations of mobile defects along with depth for the same conditions. The density of dislocation lines and diameter of grain boundaries in W are set as $10^{12}$ $m^{-2}$ and 10 $\mu m$, respectively.

diation due to the trapping of defects produced by energetic neutron; otherwise, it is nearly a diffusion type without neutron irradiation. However, for the case of lower energy ($\sim$1 $keV$) of He ions and higher temperature ($\sim$837 $K$), desorption of He in clusters from W surface becomes more obvious and thus the concentrations contributed by DLs and GBs stands out (Fig. 4(a)).

Moreover, we can further give the concentrations of different special defects (especially the mobile defects) along with depth with or without neutron irradiation by our model in detail, shown in Fig. 4(b). As expected, the concentrations for different mobile defects are directly related to their generation rates and mobilities, which fully illustrates that the trapping by other immobile defect clusters is the main absorption of mobile de-

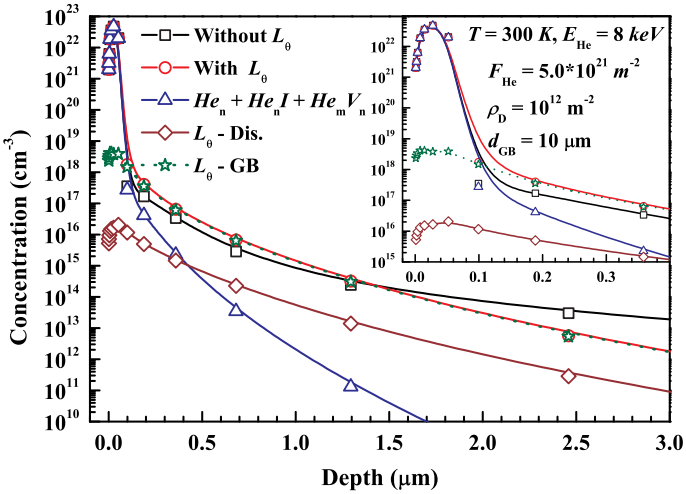


Figure 5: Depth dependence of He concentrations in W under He ions implantation with energy of 8 $keV$ and fluence of $5.0\times10^{21}$ $m^{-2}$ at 300 $K$, with/without absorption of dislocations and grain boundaries. The density of dislocation lines and diameter of grain boundaries in W are set as $10^{12}$ $m^{-2}$ and 10 $\mu m$, respectively.

fects. For the case of synergistic irradiations of ions and neutron, the depth distributions of different mobile defects are reasonable like in Fig. 4(b) after a full diffusion-absorption process, that is, most of them are located near surface due to He irradiation with high fluence, and then in equilibrium due to neutron irradiation far from surface. For the case of He ions implantation without neutron irradiation, thus most of the residual concentrations of mobile defects locate at near surface and then drop sharply when extending into deep. The concentrations of mobile defects without neutron irradiation are lower than the ones with neutron irradiation except for He atoms due to their less loss induced by intrinsic defects in the depth far from surface.

Finally, we discuss the rationality of some assumptions made in this model. As mentioned above (Fig. 4), we have concluded that the influences of inherent sinks (DLs and GBs) can not be negligible in the case of low He ions energy and high system temperature, when these sinks are prominent in some special samples. However, the discrepancy of including the influences of inherent sinks or not is vanished for the case of higher He energy (8 $keV$) and lower temperature (300 $K$), as shown in Fig. 5. He clusters dominate in the main part of He concentration due to the high damage production with higher He energy, while the concentrations by DLs and GBs are several orders lower than that by He clusters and can be neglected anyway (as performed in [69]). Moreover, the concentration of $I_2$ clusters as shown in Fig. 4(b) is negligible for the low binding energy of di-interstitial (1.02 eV). Thus, it is reasonable to neglect this term in solving Eq. (6) and then be replaced by the Fokker-Plank equation. Also, the reaction term of $I_2$ with He clusters is not important, so only the reaction of SIAs with He clusters is included as adopted in Table 1.

# 4 Conclusions

In this paper, a cluster dynamics model has been developed to account for the accumulation and diffusion processes of He atoms in W under He implantation alone/synergistic irradiation with neutron. By using this model, the concentrations of different defects with depth and size have been given for different He ions incident conditions (energies and fluences) and material conditions (system temperature and existent sinks). The calculated results agree with different experiments much well, which demonstrate that the model proposed here is very reasonable. The model has been coded as IRadMat and been applied to several typical cases, i.e., describing the He concentrations within the 2D space of defect type/size and depth, including the synergistic effect of He-neutron irradiations, taking into account of the influence of inherent sinks (dislocation lines and grain boundaries), etc. Additionally, our model would be universally used to further investigate the dynamic mechanics of defects in plasma-facing materials under ions/neutron irradiations.

# Acknowledgments

The authors are very grateful to Dr. Y. Dai of Spallation Materials Technology Spallation Neutron Source Division, Paul Scherrer Institute for his helpful comments and discussions. This work was supported by special Funds for Major State Basic Research Project of China (973) under Grant nos. 2007CB925004 and 2008CB717802, Knowledge Innovation Program of Chinese Academy of Sciences under Grant no. KJCX2-YW-N35, National Science Foundation of China under Grant no. 11005124, China Postdoctoral Science Foundation funded project under Grant no. 20100470863, and Director Grants of CASHIPS. Part of the calculations were performed in Center for Computational Science of CASHIPS.

**References**

[1] R. J. Goldston and P. H. Rutherfold. Introduction to Plasma Phys., page 156, 1996.
[2] A. Loarte, B. Lipschultz, A. S. Kukushkin, and et al. Nucl. Fusion, 47:S203–S263, 2007.
[3] M. Tokitani, N. Yoshida, M. Miyamoto, and et al. J. Nucl. Mater., 386-388:173–176, 2009.
[4] T. Hino, Y. Yamauchi, and Y. Hirohata. J. Nucl. Mater., 266-269:538–541, 1999.
[5] K. Ono, K. Arakawa, M. Oohashi, and et al. J. Nucl. Mater., 283-287:210–214, 2000.
[6] H. Iwakiri, K. Yasunaga, K. Morishita, and et al. J. Nucl. Mater., 283-287:1134–1138, 2000.
[7] K. Tokunaga, O. Yoshikawa, K. Makise, and N. Yoshida. J. Nucl. Mater., 307-311:130–134, 2002.
[8] H. Iwakiri, K. Morishita, and N. Yoshida. J. Nucl. Mater., 307-311:135–138, 2002.
[9] S. Nagata, B. Tsuchiya, T. Sugawara, and et al. J. Nucl. Mater., 307-311:1513–1516, 2002.
[10] K. Tokunaga, R. P. Doerner, R. Seraydarian, and et al. J. Nucl. Mater., 313-316:92–96, 2003.
[11] D. Nishijima, M. Y. Ye, N. Ohno, and S. Takamura. J. Nucl. Mater., 313-316:97–101, 2003.
[12] K. Tokunaga, S. Tamura, N. Yoshida, and et al. J. Nucl. Mater., 329-333:757–760, 2004.

[13] D. Nishijima, M. Y. Ye, N. Ohno, and S. Takamura. J. Nucl. Mater., 329-333:1029–1033, 2004.
[14] D. Nishijima, T. Sugimoto, H. Iwakiri, and et al. J. Nucl. Mater., 337-339:927–931, 2005.
[15] M. Tokitani, M. Miyamoto, D. Koga, and et al. J. Nucl. Mater., 337-339:937–941, 2005.
[16] N. Yoshida, H. Iwakiri, K. Tokunaga, and T. Baba. J. Nucl. Mater., 337-339:946–950, 2005.
[17] S. B. Gilliam, S. M. Gidcumb, D. Forsythe, and et al. Nucl. Instr. and Meth. in Phys. Res. B, 241:491–495, 2005.
[18] H. T. Lee, A.A. Haasz, J. W. Davis, and R. G. Macaulay-Newcombe. J. Nucl. Mater., 360:196–207, 2007.
[19] M. Tokitani, M. Miyamoto, and K. Tokunaga et al. J. Nucl. Mater., 363-365:443–447, 2007.
[20] H. T. Lee, A. A. Haasz, J. W. Davis, and et al. J. Nucl. Mater., 363-365:898–903, 2007.
[21] S. Kajita, S. Takamura, and N. Ohno. Nucl. Fusion, 47:1358–1366, 2007.
[22] K. Katayama, K. Imaoka, T. Okamura, and M. Nishikama. Fusion Eng. Des., 82:1645–1650, 2007.
[23] N. Enomoto, S. Muto, T. Tanabe, and et al. J. Nucl. Mater., 385:606–614, 2009.
[24] K. Tokunaga, T. Fujiwara, K. Ezato, and et al. J. Nucl. Mater., 390-391:916–920, 2009.
[25] Y. Watanabe, H. Iwakiri, N. Yoshida, and et al. Nucl. Instr. and Meth. in Phys. Res. B, 255:32–36, 2007.
[26] M. Samaras and M. Victoria. Materialtoday, 11:54–62, 2008.
[27] M. Samaras, M. Victoria, and W. Hoffelner. Nucl. Eng. Tech., 41:1–10, 2009.
[28] Q. Xu, N. Yoshida, and T. Yoshiie. J. Nucl. Mater., 367-370:806–811, 2007.
[29] C. S. Becquart and C. Domain. J. Nucl. Mater., 385:223–227, 2009.
[30] C. S. Becquart, C. Domain, U. Sarkar, and et al. J. Nucl. Mater., 403:75–88, 2010.
[31] A. Barbu. C. R. Physique, 9:353–361, 2008.
[32] C. J. Ortiz and M. J. Caturla. Phys. Rev. B, 75:184101, 2007.
[33] R. E. Stoller, S. I. Golubov, C. Domain, and C. S. Becquart. J. Nucl. Mater., 382:77–90, 2008.
[34] Q. Xu, K. Sato, and T. Yoshiie. J. Nucl. Mater., 390-391:663–666, 2009.
[35] E. Pollak and P. Talkner. Chaos, 15:026116, 2005.
[36] N. M. Ghoniem. Rad. Eff. Def. Sol., 148:269–318, 1999.
[37] C. J. Ortiz, M. J. Caturla, C. C. Fu, and F. Willaime. Phys. ReV. B, 80:134109, 2009.
[38] M. I. Baskes and W. D. Wilson. Phys. ReV. B, 27:2210–2217, 1983.
[39] M. F. Wehner and W. G. Wolfer. Philos. Mag. A, 52:189–205, 1985.
[40] F. Christien and A. Barbu. J. Nucl. Mater., 324:90–96, 2004.
[41] S. I. Golubov, R. E. Stoller, S. J. Zinkle, and A. M. Ovcharenko. J. Nucl. Mater., 361:149–159, 2007.
[42] M. P. Surh, J. B. Sturgeon, and W. G. Wolfer. J. Nucl. Mater., 378:86–97, 2008.
[43] N. M. Ghoniem and S. Sharafat. J. Nucl. Mater., 92:121–135, 1980.
[44] M. P. Surh, J. B. Sturgeon, and W. G. Wolfer. J. Nucl. Mater., 325:44–52, 2004.
[45] C. Pokor, Y. brechet, P. Dubuisson, and et al. J. Nucl. Mater., 326:19–29, 2004.
[46] E. Meslin, A. Barbu, L. Boulanger, and et al. J. Nucl. Mater., 382:190–196, 2008.
[47] F. Christien and A. Barbu. J. Nucl. Mater., 393:153–161, 2009.
[48] A. Hardouin Duparc, C. Moingeon, N. Smetniansky de Grande, and A. Barbu. J. Nucl. Mater., 302:143–155, 2002.
[49] F. Christien and A. Barbu. J. Nucl. Mater., 346:272–281, 2005.
[50] A. Gokhman and F. Bergner. Radiat. Eff. Defects Solids, 165:216–226, 2010.
[51] C. J. Ortiz, M. J. Caturla, C. C. Fu, and F. Willaime. Phys. Rev. B, 75:100102, 2007.
[52] C. J. Ortiz, M. J. Caturla, C. C. Fu, and F. Willaime. J. Nucl. Mater., 386-388:33–35, 2009.
[53] H. Trinkaus and B. N. Singh. J. Nucl. Mater., 323:229–242, 2003.

[54] Y. G. Li, W. H. Zhou, H. L. Feng, Z. Zeng, and X. Ju. Cluster dynamics modeling of accumulation and diffusion of helium in neutron irradiated tungsten. Unpublished.
[55] J. P. Biersack and L. G. Haggmark. Nucl. Instrum. Methods, 174:257–269, 1980; TRIM/SRIM website, `http://www.srim.org`.
[56] A. A. Turkin and A. S. Bakai. J. Nucl. Mater., 358:10–25, 2006.
[57] B. Neta. Numerical Solution of Partial Differential Equations MA 3243 Lecture Notes. Unpublished, California, 2003.
[58] L. R. Petzold. Siam J. Sci. Stat. Comput., 4:136–148, 1983.
[59] G. Federici, J. N. Brooks, D.P. Coster, and et al. J. Nucl. Mater., 290-293:260–265, 2001.
[60] J. Fikar and R. Schaublin. Nucl. Instr. Methods Phys. Res. B, 267:3218–3222, 2009.
[61] G. E. Dieter. Mechanical Metallurgy. McGraw-Hill Book Company, London, si metric edition, 1988.
[62] P. A. T. Olsson. Compu. Mater. Sci., 47:135–145, 2009.
[63] A. E. Carlsson. Solid State Phys., 43:1–91, 1990.
[64] P. M. Derlet, D. Nguyen-Manh, and S. L. Dudarev. Phys. Rev. B, 76:054107, 2007.
[65] C. S. Becquart and C. Domain. Nucl. Instr. Methods Phys. Res. B, 255:23–26, 2007.
[66] C. S. Becquart and C. Domain. Phys. Rev. Lett., 97:196402, 2006.
[67] T. Ahlgren, K. Heinola, N. Juslin, and A. Kuronen. J. Appl. Phys., 107:033516, 2010.
[68] T. Ono, T. Kawamura, T. Kenmotsu, and Y. Yamamura. J. Nucl. Mater., 290-293:140–143, 2001.
[69] Y. G. Li, W. H. Zhou, H. L. Feng, N. R. Hui, Z. Zeng, and X. Ju. Accumulation of he on w surface during kev-he irradiation: A cluster dynamics modeling. Unpublished.